Published on 14 September 2016. Downloaded by Saint Petersburg State University of IT Mechanics and Optics on 7/18/2024 11:12:59 AM.

Nanoscale

ROYAL SOCIETY OF CHEMISTRY

PAPER

View Article Online
View Journal | View Issue

Cite this: *Nanoscale*, 2016, **8**, 17809

Self-adjusted all-dielectric metasurfaces for deep ultraviolet femtosecond pulse generation†

S. V. Makarov,*[a] A. N. Tsypkin,[a] T. A. Voytova,[a] V. A. Milichko,[a] I. S. Mukhin,[a,b] A. V. Yulin,[a] S. E. Putilin,[a] M. A. Baranov,[a] A. E. Krasnok,[a] I. A. Morozov[b] and P. A. Belov[a]

Received 16th June 2016,
Accepted 9th September 2016

DOI: 10.1039/c6nr04860a

www.rsc.org/nanoscale

The advantage of metasurfaces and nanostructures with a high nonlinear response is that they do not require phase matching, and the generated pulses are short in the time domain without additional pulse compression. However, the fabrication of large-scale planar structures by lithography-based methods is expensive, time consuming, and requires complicated preliminary simulations to obtain the most optimized geometry. Here, we propose a novel strategy for the self-assembled fabrication of large-scale resonant metasurfaces, where incident femtosecond laser pulses adjust the initial silicon films *via* specific surface deformation to be as resonant as possible for a given wavelength. The self-adjusting approach eliminates the necessity of multistep lithography and designing, because interference between the incident and the scattered parts of each laser pulse "imprints" resonant field distribution within the film. The self-adjusted metasurfaces demonstrate a high damage threshold (≈10^{12} W cm^{-2}) and efficient frequency conversion from near-IR to deep UV. The conversion efficiency is up to 30-fold higher compared with nonresonant smooth Si films. The resulting metasurfaces allow for the generation of UV femtosecond laser pulses at a wavelength of 270 nm with a high peak and average power (≈10^5 W and ≈1.5 μW, respectively). The results pave the way to the creation of ultrathin nonlinear metadevices working at high laser intensities for efficient deep UV generation at the nanoscale.

1 Introduction

Highly efficient generation of deep (100–280 nm) ultraviolet (UV) ultrashort pulses is a highly important issue for time-domain fluorescence spectroscopy, photo-therapy, and nanolithography.[1–4] Third harmonics generation (THG) is one of the most promising strategies to achieve deep UV wavelengths. Among different approaches, ultrathin metasurface-based nonlinear frequency converters have attracted special interest owing to the needlessness of phase-matching or compensation of group-velocity dispersion, whereas enhancement of the local optical field leads to a higher UV yield.[5] Moreover, each metaatom of a nonlinear metasurface is a nanoscale source of UV light, which is useful for extremely localized and selective exposition of different nanoobjects. In particular, the nonlinear response of plasmonic nanostructures and metasurfaces has been extensively studied to achieve highly effective harmonics generation.[5–9] However, the efficiency of nonlinear frequency conversion in metallic nanoparticles is strongly limited by their high optical losses and relatively low damage thresholds (about 10^{10} W cm^{-2}) compared to dielectrics. In turn, all-dielectric nanostructures and metasurfaces based on resonant dielectric nanoparticles with a high refractive index have emerged as promising objects for nonlinear nanophotonics,[10–16] being much more compact compared with the conventional dielectric microdevices.[17,18] Among different dielectrics, silicon can be considered as one of the most promising materials for nonlinear all-dielectric nanophotonics, owing to its high nonlinear susceptibility and low-losses in the visible range.[10,13,18]

An additional important parameter for the optimisation of harmonics generation from resonant nanoparticles is a thermal sink, which can sufficiently increase the damage threshold of the nanoparticles.[19] From this point of view, it is more reasonable to use nanostructured homogeneous materials rather than nanoparticle-based metasurfaces, when their supporting substrate is a bad thermal conductor (silica, sapphire, *etc.*). Previously reported non-lithographic methods for effective large-scale Si nanoparticle fabrication[20–23] can be hardly integrated with an effective thermal sink, whereas widespread lithography-based methods are time-consuming, expensive, and require a specific design.

[a]*ITMO University, St. Petersburg 197101, Russia. E-mail: s.makarov@metalab.ifmo.ru*
[b]*St. Petersburg Academic University, St. Petersburg 194021, Russia*

† Electronic supplementary information (ESI) available. See DOI: 10.1039/C6NR04860A

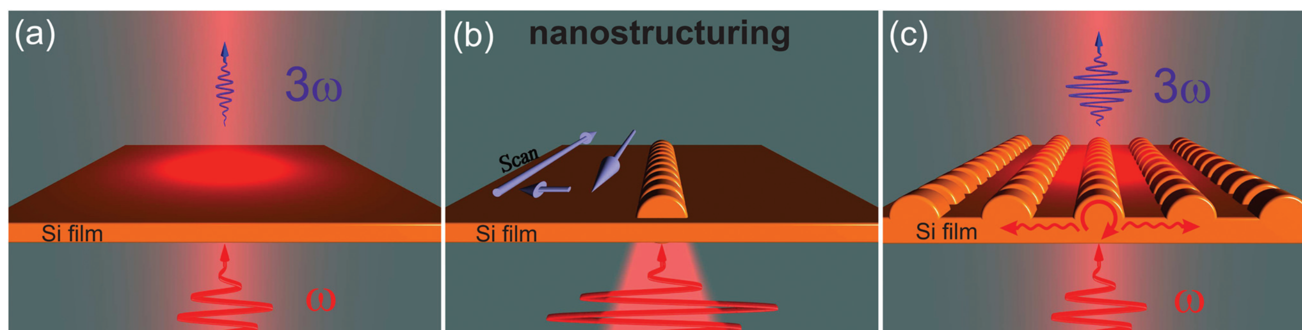

Fig. 1 Schematic sketches of third harmonic generation from (a) smooth and (c) nanostructured Si film. (b) Principle of Si film laser-induced nanostructuring.

Published on 14 September 2016. Downloaded by Saint Petersburg State University of IT Mechanics and Optics on 7/18/2024 11:12:59 AM.

In this paper, we propose a novel strategy to enhance the generation efficiency of highly intense deep UV pulses of ultrashort duration by means of laser-induced self-organized nanostructuring of thin Si films. The resonant response of the fabricated Si nanostructures (metasurfaces) is achieved at a certain thickness of the Si film when incident laser pulses can excite a waveguide mode interfering with the incident field, resulting in ultrafast periodic heating and film deformation. This approach provides a resonant optical response of the metasurface at a pumping wavelength and an excellent thermal sink, simultaneously. Our method eliminates the necessity to carry out a specific design of the metasurface, because the laser-induced self-organisation mechanism is based on the interference between the incident laser field and the resonant waveguide mode. Thus, the resulting metasurface is always self-adjusted to provide the maximum energy deposition for the used laser wavelength, enabling fabrication of a metasurface and generation of UV pulses from it by using exactly the same setup. The self-adjusted metasurfaces demonstrate up to a 30-fold increase of the THG efficiency compared with thicker nonresonant Si films and 2.5-fold enhancement compared with an initial film supporting a Fabry–Perot resonance. The proposed method allows for the application of high intensities (up to 80 GW cm^{-2}) to effectively generate deep UV laser pulses. The principle of THG enhancement *via* Si film laser nanostructuring is depicted in Fig. 1.

2 Results and discussion

2.1 Sample fabrication

In order to develop a novel method of all-dielectric metasurface fabrication *via* femtosecond laser irradiation of a-Si:H films, we carried out optimization experiments revealing the strong dependence on the film thickness (for details, see section I in the ESI†). The experimental parameters used for the fabrication are given in the Experimental section. A thickness of 100 nm corresponds to the most reproducible metasurface formation, which is shown in Fig. S1.† The resulting metasurface represents a periodic array of nanobumps with mean periods ≈260 nm along one axis and ≈700 nm along the perpendicular axis, the width of the bumps being ≈130 nm and the length being ≈330 nm (Fig. 2a). The 700 nm period is equal to the scanning period of the laser nanostructuring. All dimensions of the metasurface are smaller than the wavelength of the fs-laser (800 nm) and the whole visible spectrum.

The physical mechanism of the metasurface formation under multipulse irradiation is the interference of the incident laser field with the electric field of the wave propagating in the film and the following selective film melting and deformation. The mode in the film can be excited *via* scattering on random

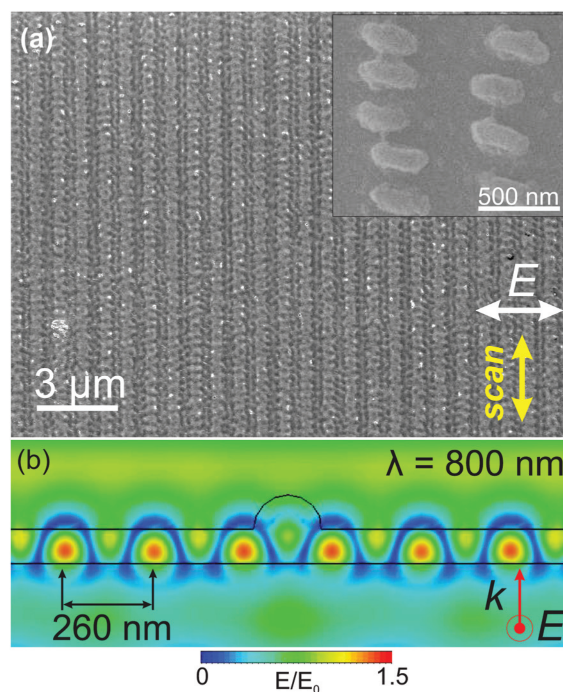

Fig. 2 (a) SEM image of a self-organized Si metasurface. Inset: zoomed part of the metasurface. (b) Calculated value of the total electric field (averaged over time) near a subwavelength hemispherical feature on a 100 nm Si film after incidence of a plane electromagnetic wave.

This journal is © The Royal Society of Chemistry 2016

Published on 14 September 2016. Downloaded by Saint Petersburg State University of IT Mechanics and Optics on 7/18/2024 11:12:59 AM.

roughness, which is formed after several first laser pulses. Due to the ultrashort pulse duration, one can neglect the thermal effects during the interference laser energy deposition and describe the resulting nanostructure morphology in terms of an electrodynamic approach. However, analytical modeling based on the widely acknowledged Sipe's model[24] does not provide quantitative prediction of the distance between the nanoparticles within the metasurface, because it does not take into account the film thickness (for details of the calculations, see section II in the ESI†). As shown in Fig. 2b, full-wave numerical simulation using the CST Microwave Studio reveals the formation of the standing wave at λ = 800 nm around an arbitrary nanofeature with a period of around 260 nm, which is close to the measured values. In particular, we observe coupling of a normally incident laser wave to a planar waveguide mode within the Si film. This coupled waveguide mode interferes with the incident field, providing the formation of a standing wave within the film and modulated heating with a period of about 260 nm. The electric field enhancement within each maximum is about 1.5, resulting in ultrafast non-uniform heating and deformation of the film due to thermal expansion and fast resolidification.

The experimental reflection spectrum of the self-adjusted metasurface exhibits considerable differences compared to the reflectance spectrum of the initial film (Fig. 3a). In particular, we observe specific spectral features in the vicinity of 800 nm, *i.e.* exactly near the wavelength of the femtosecond laser pulses. Our numerical modeling of reflectance for this case exhibits good agreement with the corresponding experimental measurements. Since there is a relatively broad maximum in the spatial Fourier spectrum of the metasurface (Fig. S2a†), our numerical calculations take into account the deviations of the period as 260 ± 30 nm, where all the obtained theoretical spectra are averaged. The averaging of the spectra is carried out as summation of all the numerically calculated spectra for the periods in the range of 230–290 nm with a 5 nm step, and dividing this sum by 13. According to our near-field calculations, this peak corresponds to a strong (up to 7 times) electric field enhancement (Fig. 3d) compared to the smooth film with the same thickness (Fig. 3c). The calculated electric field distribution in Fig. 3d proves that such an enhancement is caused by an excitation of a magnetic-like dipole mode (or TM-mode) within each nanoparticle. Importantly, this TM-mode has a ring-like field structure, where the local minimum is in the center of the nanoparticle and the local maximum is shifted to the surface.

As a result of such laser multipulse nanostructuring, the irradiated film is covered by the resonant nanoparticles with a certain period, which enables maximal laser energy deposition for the used laser wavelength.[24] Indeed, the spectral width of the laser pulses applied for nanostructuring (≈28 nm, see section III in the ESI†) is close to the width of the optical resonance of the nanostructure (≈28 nm, see Fig. 3a). It means that the proposed method offers fabrication of a metasurface self-adjusted to the incident laser wavelength. The advantage of this approach is that no efforts to design the shape of the resonant metasurface are needed, and the existence of the resonance is provided by the fabrication method.

2.2 UV pulse generation

Since the self-adjusted metasurface exhibits resonance properties near 800 nm with an enhanced electric field within silicon, it should enhance THG around a wavelength of 270 nm, *i.e.* in the UV range where bulk Si is opaque. Filtered and measured UV signals can be clearly seen by using a spectrometer (for measurement details, see the Experimental section), excluding the influence of the possible one-photon or multiphoton luminescence. A smooth Si film, supporting the Fabry–Perot resonance at 800 nm and the formation of the resonant metasurface, shows a sharp maximum of the UV signal at 100–120 nm thicknesses (Fig. 4a). The largest difference in the THG signal is observed between 170 nm and 100 nm films, giving a 15-fold enhancement.[25]

In Fig. 4b, the comparison of the UV signal from the metasurface with the UV signal from the thin 100 nm film is presented, revealing a 2.5-fold enhancement of the third-harmonics conversion efficiency and the 30-fold enhancement compared to the nonresonant 170 nm film. It is worth noting

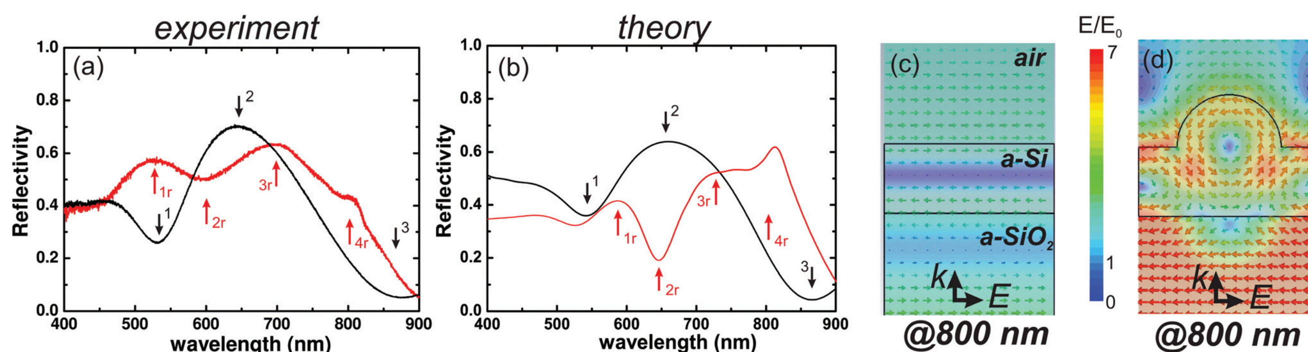

Fig. 3 Experimental (a) and theoretical (b) reflection spectra of initial (black curve), and nanostructured (red curve) Si films with 100 nm thickness on infinite fused silica. The arrows in figures (a) and (b) point to the positions of the resonances. Numerically calculated normalized field intensity distribution near initial (c) and nanostructured (d) Si films with 100 nm thickness on an infinite fused silica.

Published on 14 September 2016. Downloaded by Saint Petersburg State University of IT Mechanics and Optics on 7/18/2024 11:12:59 AM.

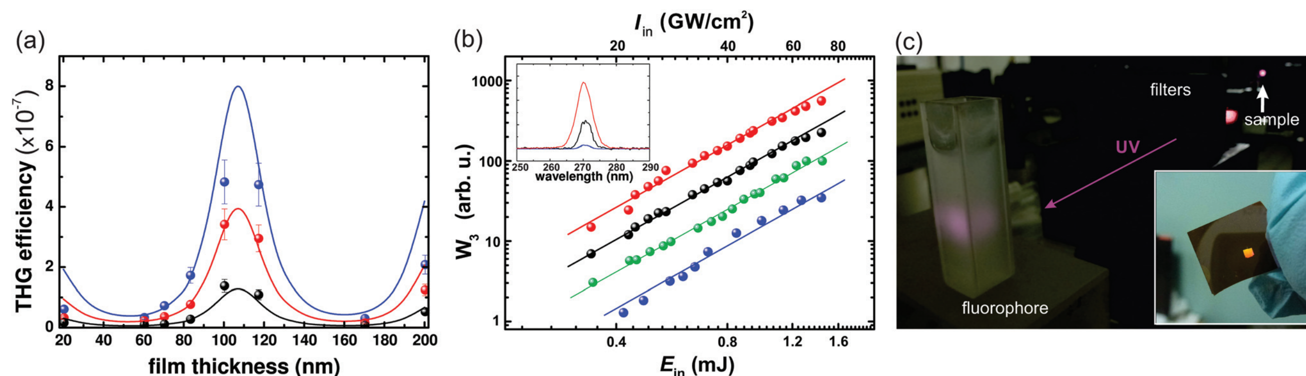

Fig. 4 (a) Experimental (circles) and theoretical (lines) dependencies of third harmonic generation (THG) efficiency on Si film thickness at various pump intensities: 20 GW cm^{-2} (black), 35 GW cm^{-2} (red), 55 GW cm^{-2} (blue). (b) Experimental dependencies of third harmonic intensity from initial (black dots) and nanostructured Si films with 100 nm thickness on a fused silica substrate with resonant (red dots) and non-resonant (green dots) geometry. Third harmonics signals from a smooth 170 nm Si film (blue dots). All approximation lines correspond to the 2.8 ± 0.2 slope. Inset: spectral range in the vicinity of the third harmonic signal. (c) Photography of fluorescence induced by the generated UV light in a fluorophore (strontium aluminate doped with europium and dysprosium). Inset: view of the sample with a self-organized metasurface (orange area).

that the UV signal was measured in zero diffraction order, whereas +1 and −1 diffraction orders of UV light propagate at nearly grazing angles and can be seen by the naked eye. The comparison of the metasurfaces with different periods reveals that the UV output signal from the resonant metasurface (with a period of 270 nm) is one order of magnitude stronger than the output signal from the non-resonant samples (with a period of 400 nm), see Fig. 4b. A similar behavior is observed if the metasurface resonant for a wavelength of 800 nm is irradiated by fs-laser pulses at different wavelengths. The details of the non-resonant nanostructure fabrication and characterization are presented in section IV in the ESI.†

A high peak power of the output pulses was achieved by using a low-repetition rate (1 kHz) for irradiation of the large-scale self-organized metasurface (≈0.6 cm^2). We used 800 nm laser pulses with energies up to 1.5 mJ diaphragmed to 8 mm diameter on the $1/e$ intensity level. The observed maximum TH conversion efficiency is about 0.9×10^{-6} for the 100 nm film and the incident pulse energy of 1.5 mJ. The conversion efficiency is determined as $\eta = W_3/W_1$, where W_3 and W_1 are third-harmonic and incident energies, respectively.

In our experiments, the maximum laser intensity is about 80 GW cm^{-2} (F = 3 mJ cm^{-2} for 40 fs), which is much smaller than the damage threshold of a Si film (100 mJ cm^{-2})[23] and around the level of dense electron–hole plasma generation (F > 1 mJ cm^{-2}).[10–13] Although the conversion efficiency for our system is not a record among the previously reported values achieved in high-Q resonators,[13,18] the measured output energies and the average power of UV femtosecond laser pulses are much larger. Indeed, the advantage of our systems is that they allow for working with a much more powerful pump and generating UV femtosecond pulses with the energy as high as W_3 = 1.3 nJ per pulse. This value is several orders of magnitude higher than that reported for all-dielectric[10,13] and plasmonic[5,26] nanostructures and metasurfaces. Moreover, our method gives similar efficiencies at the corresponding intensities reported for THG in ZnO films[27] and for advanced organic–inorganic materials.[28] It yields a high average power of a femtosecond UV beam of about $P_{av} \approx 1.5$ μW, being high enough to provide visible fluorescence of strontium aluminate doped with europium and dysprosium in a quartz cuvette, as demonstrated in Fig. 4c. The peak power of the generated UV fs-laser pulses can be estimated as $P_{peak} = W_3/\tau_3 = (W_3\Delta\lambda c)/(K\lambda^2)$, where c is the light velocity, $\Delta\lambda$ is the spectral width of a UV femtosecond laser pulse, and K is the constant which determines the time–bandwidth product (K = 0.441 for a Gaussian pulse). The maximum estimated peak power of the UV pulse is up to $P_{peak} \sim 10^5$ W at the following parameters: W_3 = 1.3 nJ, $c = 3 \times 10^8$ m s^{-1}, $\Delta\lambda$ = 7 nm, and λ = 270 nm. The pulse duration τ_3 of the UV pulse at such parameters taking into account material dispersion and the effect of the resonator is estimated to be less than 30 fs (for details of calculations, see section V in the ESI†).

The experimental results can be described in terms of excitation of modes within a film or nanostructure. The energy of the emitted third harmonic W_3 from the unit square of the surface can be expressed through the integral of the product of the Green function $G(x)$ and the nonlinear current $j_n(x)$ over the film or nanostructure thickness d:

$$W_3 \sim |E_3|^2 = \left|\int_0^d G(x) j_n(x) \mathrm{d}x\right|^2. \quad (1)$$

In turn, the nonlinear current can be expressed as $j_n = \chi^{(3)} \cdot E_1{}^3$, where E_1 is the electric field at the fundamental frequency and $\chi^{(3)}$ is the nonlinear susceptibility. From expression (1) it is clearly seen that the efficiency of the third harmonic generation depends not only on the intensity distribution of the nonlinear current $j_n(x)$ but also on the Green function $G(x)$, which characterizes the resonances of the structure. Thus, the resonances on the frequency of the third harmonic can also enhance the emission of the radiation.

 This journal is © The Royal Society of Chemistry 2016

Published on 14 September 2016. Downloaded by Saint Petersburg State University of IT Mechanics and Optics on 7/18/2024 11:12:59 AM.

However, for the experimental conditions, the losses are high at the frequency of the third harmonic and, thus only the radiation from a thin layer close to the interface is important.

Note that due to experimental convenience, we normalized the third harmonic on the transmitted first harmonic intensity. Fig. 4a shows the dependencies of η on the film thickness calculated by using formula (1) using the Green function rigorously calculated for the planar structure (for details of calculations, see section VI in the ESI†). The fundamental field distribution cannot be found analytically for the real geometry. The simulations show that there are resonances causing enhancement of the electric field of the fundamental harmonic (Fig. 3d). The numerical simulations allow one to obtain an accurate description of the fields excited in the structure, yielding a 5-fold average enhancement of the electric field in the sub-surface layer with a thickness of about 10 nm, whereas the corresponding value for the smooth 100 nm film is about 2.5 (Fig. 3c), resulting in THG enhancement $(|E_3|/|E_1|)^6 \approx 64$. In our experiments, we observed lower values of enhancement due to the specificity of the detection scheme measuring THG only in the forward direction losing scattered signals. The field enhancement in such a thin sub-surface layer is crucial, because the generated 270 nm UV light has a propagation length of about 10 nm through silicon. In this case, the most effective contribution to the integration in eqn (1) gives this 10 nm sub-surface layer. From this it follows that for efficient third harmonic generation the field of the fundamental mode must have the highest possible intensity in the vicinity of the silicon interfaces. Transversal magnetic ring-like modes have the intensity maxima at the surfaces of the silicon film and that is why the modes of this kind are the best for the generation of UV light at silicon metasurfaces.

3 Conclusion

In summary, we have applied self-organized laser-induced nanostructuring of thin Si films to fabricate all-dielectric metasurfaces, which provides a resonance optical response at a pumping wavelength for third-harmonic generation. The fabrication method is a single-step, vacuum-free, and mask-free approach with no chemical etching or other post-processing procedures. Moreover, it is extremely convenient, because one does not need to develop a specific design of a metasurface for the strongest field enhancement. The self-adjusted metasurface has demonstrated a 2.5-fold enhancement of THG compared with an initial film with the highest conversion efficiency. This allows one to achieve the generation of UV radiation at the wavelength of 270 nm with a high peak and average power (10^5 kW and 1.5 μW, correspondingly). According to the spectral width of the UV pulses, their duration is shorter than 30 fs. Such a high peak power from the ultrathin metasurface makes the generated UV pulses applicable in a wide range of applications: high-resolution photolithography, deep-UV photoexcitation for time-resolved measurements *etc*. Additionally, the ultrathin thickness of the nonlinear metasurfaces is extremely promising for further development of novel autocorrelation techniques.[29]

4 Experimental section

4.1 Metasurface fabrication

a-Si:H films with thicknesses in the range of 20–200 nm were deposited on a substrate of fused silica by plasma enhanced chemical vapor deposition from SiH_3 precursor gas (an initial hydrogen concentration ~10% was used). The film irradiation is carried out by focusing fs-laser pulses (100 fs) into 0.9 μm spots at the $1/e$ level through a NA = 0.75 objective. Surface scanning by the focused beam with 0.11 J cm^{-2}, repetition rate 10 kHz, and scan speed 20 μm s^{-1} provides ≈450 absorbed laser pulses per spot. Increasing of the repetition rate will make this nanostructuring process applicable for wafer-scale fabrication.

4.2 THG generation

For THG a commercial femtosecond laser system (based on a Ti:sapphire regenerative amplifier Regulus 35F1K, Avesta Project) was used. Laser pulses have 800 nm central wavelength, with a maximum pulse energy of 2 mJ, and a pulse duration of 40 fs at a repetition rate of 1 kHz. Laser energy was varied and controlled by using a polarising filter and a power meter (Nova II, Ophir), respectively, while the pulse duration was measured by using an autocorrelator ASF-20 (Avesta Project). The THG signal was separated from the fundamental wavelength by using a set of filters and measured by using the power meter. All measurements of THG were carried out in zero diffraction order in the far field to provide the values for useful signals. Additional measurements of the TH power carried out in two diffraction orders reveal at least 40% of the value for zero order. Therefore, the measured conversion efficiency is always much less than it can be estimated from the numerical calculations of the electric field inside the films.

4.3 Characterization

High-resolution morphology characterization was carried out by means of a scanning electron microscope (SEM, Carl Zeiss, Merlin) and an atomic force microscope (AFM, SmartSPM AIST-NT). The Fourier spectra of SEM images were obtained using ImajeJ software. Optical transmission (T) and reflection (R) broadband measurements were carried out at the normal incidence of linearly polarized light from a halogen lamp (HL-2000-FHSA), using a commercial spectrometer (Horiba LabRam HR) with a CCD camera (Andor DU 420A-OE 325). The excitation Olympus PlanFI (NA = 0.95) and collection Mitutoyo M Plan APO NIR (NA = 0.7) objectives were used for transmission measurements. The objective Mitutoyo M Plan APO NIR (NA = 0.42) was employed for reflection measurements.

View Article Online

Published on 14 September 2016. Downloaded by Saint Petersburg State University of IT Mechanics and Optics on 7/18/2024 11:12:59 AM.

4.4 Numerical simulation

Numerical simulations are performed by using a time-domain solver in the commercial software CST Microwave Studio. The incidence of a plane wave at a given wavelength on an a-Si[30] film of a given thickness on a semi-infinite fused silica (ε_{SiO_2} = 2.1) substrate is considered.

Authors contribution

S. V. M., A. N. T., V. A. M., and S. E. P. conducted the optical experiments. I. S. M., M. A. B., I. A. M., and S. V. M. fabricated the samples and characterized them. T. A. V., A. V. Y., and S. V. M. carried out the theoretical analysis and developed the interpretation with the help of A. E. K. S. V. M. wrote the paper with the help of A. V. Y. and A. E. K. P. A. B. supervised the project.

Conflict of interest

The authors declare no competing financial interest.

Acknowledgements

This work was financially supported by the Russian Science Foundation (Grant 15-19-30023). S. V. Makarov and A. V. Yulin are thankful to the ITMO Fellowship Program. We are grateful to A. V. Vinogradov and V. V. Vinogradov for providing doped strontium aluminate.

References

1 E. C. Friedberg, *Nature*, 2003, **421**, 436–440.
2 J. R. Lakowicz, *Principles of fluorescence spectroscopy*, Springer Science & Business Media, 2013.
3 J. Andres, R. D. Hersch, J.-E. Moser and A.-S. Chauvin, *Adv. Funct. Mater.*, 2014, **24**, 5029–5036.
4 S. R. Panikkanvalappil, S. M. Hira and M. A. El-Sayed, *Chem. Sci.*, 2016, **7**, 1133–1141.
5 A. E. Minovich, A. E. Miroshnichenko, A. Y. Bykov, T. V. Murzina, D. N. Neshev and Y. S. Kivshar, *Laser Photonics Rev.*, 2015, **9**, 195–213.
6 M. Kauranen and A. Zayats, *Nat. Photonics*, 2012, **6**, 737–748.
7 P. M. Schwab, C. Moosmann, M. D. Wissert, E. W.-G. Schmidt, K. S. Ilin, M. Siegel, U. Lemmer and H.-J. Eisler, *Nano Lett.*, 2013, **13**, 1535–1540.
8 H. Aouani, M. Rahmani, M. Navarro-Cía and S. A. Maier, *Nat. Nanotechnol.*, 2014, **9**, 290–294.
9 M. Mesch, B. Metzger, M. Hentschel and H. Giessen, *Nano Lett.*, 2016, **16**(5), 3155–3159.
10 M. R. Shcherbakov, D. N. Neshev, B. Hopkins, A. S. Shorokhov, I. Staude, E. V. Melik-Gaykazyan, M. Decker, A. A. Ezhov, A. E. Miroshnichenko, I. Brener, A. A. Fedyanin and Y. S. Kivshar, *Nano Lett.*, 2014, **14**, 6488–6492.
11 S. Makarov, S. Kudryashov, I. Mukhin, A. Mozharov, V. Milichko, A. Krasnok and P. Belov, *Nano Lett.*, 2015, **15**, 6187–6192.
12 M. R. Shcherbakov, P. P. Vabishchevich, A. S. Shorokhov, K. E. Chong, D.-Y. Choi, I. Staude, A. E. Miroshnichenko, D. N. Neshev, A. A. Fedyanin and Y. S. Kivshar, *Nano Lett.*, 2015, **15**, 6985–6990.
13 Y. Yang, W. Wang, A. Boulesbaa, I. I. Kravchenko, D. P. Briggs, A. Puretzky, D. Geohegan and J. Valentine, *Nano Lett.*, 2015, **15**, 7388–7393.
14 T. Lewi, P. P. Iyer, N. A. Butakov, A. A. Mikhailovsky and J. A. Schuller, *Nano Lett.*, 2015, **15**, 8188–8193.
15 L. Carletti, A. Locatelli, O. Stepanenko, G. Leo and C. De Angelis, *Opt. Express*, 2015, **23**, 26544–26550.
16 D. G. Baranov, S. V. Makarov, V. A. Milichko, S. I. Kudryashov, A. E. Krasnok and P. A. Belov, 2016, arXiv:1603.04397.
17 B. Corcoran, C. Monat, C. Grillet, D. J. Moss, B. J. Eggleton, T. White, L. O'Faolain and T. F. Krauss, *Nat. Photonics*, 2009, **3**, 206–210.
18 J. Leuthold, C. Koos and W. Freude, *Nat. Photonics*, 2010, **4**, 535–544.
19 P. N. Melentiev, A. E. Afanasiev, A. A. Kuzin, V. M. Gusev, O. N. Kompanets, R. O. Esenaliev and V. I. Balykin, *Nano Lett.*, 2016, **16**(2), 1138–1142.
20 L. Shi, T. U. Tuzer, R. Fenollosa and F. Meseguer, *Adv. Mater.*, 2012, **24**, 5934–5938.
21 P. Moitra, B. A. Slovick, W. Li, I. I. Kravchencko, D. P. Briggs, S. Krishnamurthy and J. Valentine, *ACS Photonics*, 2015, **2**, 692–698.
22 M. Abbarchi, M. Naffouti, B. Vial, A. Benkouider, L. Lermusiaux, L. Favre, A. Ronda, S. Bidault, I. Berbezier and N. Bonod, *ACS Nano*, 2014, **8**, 11181–11190.
23 P. Dmitriev, S. V. Makarov, V. Milichko, I. Mukhin, A. Gudovskikh, A. Sitnikova, A. Samusev, A. Krasnok and P. Belov, *Nanoscale*, 2015, **8**, 5043–5048.
24 J. Sipe, J. F. Young, J. Preston and H. Van Driel, *Phys. Rev. B: Condens. Matter*, 1983, **27**, 1141.
25 P. N. Saeta and N. Miller, *Appl. Phys. Lett.*, 2001, **79**, 2704–2706.
26 J. Reinhold, M. Shcherbakov, A. Chipouline, V. Panov, C. Helgert, T. Paul, C. Rockstuhl, F. Lederer, E.-B. Kley, A. Tünnermann, *et al.*, *Phys. Rev. B: Condens. Matter*, 2012, **86**, 115401.
27 G. Petrov, V. Shcheslavskiy, V. Yakovlev, I. Ozerov, E. Chelnokov and W. Marine, *Appl. Phys. Lett.*, 2003, **83**, 3993–3995.
28 M. Liu, H. S. Quah, S. Wen, Z. Yu, J. J. Vittal and W. Ji, *Chem. Mater.*, 2016, **28**, 3385–3390.
29 S. K. Das, C. Schwanke, A. Pfuch, W. Seeber, M. Bock, G. Steinmeyer, T. Elsaesser and R. Grunwald, *Opt. Express*, 2011, **19**, 16985–16995.
30 E. D. Palik, *Handbook of optical constants of solids*, Academic press, 1998.

This journal is © The Royal Society of Chemistry 2016